Journal Name

ARTICLE

Electromagnetic wave absorption properties of ternary poly(vinylidene fluoride)/magnetite nanocomposites with carbon nanotubes and graphene

Received 00th January 20xx,
Accepted 00th January 20xx

DOI: 10.1039/x0xx00000x

www.rsc.org/

C. Tsonos,[a,b †] N. Soin,[b] G. Tomara,[c] B. Yang,[d] G. C. Psarras,[e] A. Kanapitsas[a] and E. Siores[b]

Ternary nanocomposite systems of poly(vinylidene fluoride)/magnetite/carbon nanotube (PVDF/Fe_3O_4/CNT) and poly(vinylidene fluoride)/magnetite/graphene (PVDF/Fe_3O_4/GN), were prepared using high shear twin screw compounding followed by compression moulding. The electromagnetic (EM) microwave absorption properties of the nanocomposites were investigated in the frequency range of 3-10 GHz. PVDF/Fe_3O_4/CNT samples with thickness *d* = 0.7 mm presents a minimum reflection loss (*RL)* -28.8 dB at 5.6 GHz, while all the *RL* values in the measurement frequency range 3-10 GHz are lower than -10 dB. PVDF/Fe_3O_4/GN with thickness 0.9 mm, presents a minimum *RL* of -22.6 dB at 5.4 GHz, while all the *RL* values in the measurement frequency range 3-10 GHz are lower than -10 dB as well. The excellent microwave absorption properties of both nanocomposites, in terms of minimum *RL* value and the broad absorption bandwidth**,** are mainly due to the enhanced magnetic losses. The results indicate that the ternary nanocomposites studied here, can be used as an attractive candidate for EM absorption materials in diverse fields of various technological applications, not only in the frequency range 3-10 GHz, but also at frequencies <3 GHz for PVDF/Fe_3O_4/CNT and >10 GHz for PVDF/Fe_3O_4/GN with realistic thin thickness of close to 1 mm.

Introduction

In recent years, devices using high frequency electromagnetic (EM) waves have been drawing attention, due to the exponential growth in their utilization in electronic devices for telecommunication, industrial, medical and other applications [1]. In addition, there are ongoing controversies worldwide over the potential health hazards to the human body associated with long-term exposure to electromagnetic fields. Hence, considerable attention is being given to the development of novel EM wave absorption materials [2-4]. For the production of broadband high EM wave absorbing materials, several parameters needed to be taken into consideration such as weight, thickness, types and content of filler, environmental resistance, mechanical strength and thermal stability [5]. The combination of polymers and nanomaterials is one of the most suitable methods to integrate inorganic materials with high electric and/or magnetic losses, with the advantages of flexibility and ease of processing of polymers to design excellent EM wave absorbers [6]. These nanocomposites provide merits of light weight, flexibility and cost effectiveness. For polymer matrix, there are various options such as polyaniline (PANI), polypyrrole (PPy) and poly(vinylidene fluoride) (PVDF), which have been extensively used for the manufacture of microwave absorbers [7-9]. Ferrites [10], spinel-type ferrites [11], and metallic magnetic materials [12] are the typical magnetic nanomaterials inclusions which have been widely studied. Over the past few years, magnetite (Fe_3O_4) with its dual dielectric and magnetic loss properties in the microwave region has been investigated for EM wave attenuation properties, however, Fe_3O_4 nanoparticles used in microwave absorbers suffer from narrow absorption in the low-frequency range, ease of oxidation and the need for high loading (above 50 wt.%) [10]. To overcome this, conducting nanomaterial inclusions such as one dimension carbon nanotubes (CNT) [13] and two dimension graphene (GN) [7] with low density and high complex permittivity values have been recently investigated as a promising candidate for microwave absorbers. Among these systems, the Fe_3O_4-carbon based materials are particularly interesting owing to synergistic and complementary behaviour between the magnetic and dielectric losses. In fact, previous studies on the carbon encapsulated Fe_3O_4/PVDF, Fe_3O_4-graphene and Fe_3O_4-carbon nanotube composites have reported on the excellent EM shielding behaviour of these materials [15-17]. In polymer-based magnetic nanocomposites, strong electronic interactions between magnetic nanoparticles and polymer

[a] Electronics Engineering Department, Technological Educational Institute (TEI) of Sterea Ellada, 35100 Lamia, Greece
[b] Institute for Materials Research and Innovation (IMRI), University of Bolton, Deane Road, Bolton BL3 5AB, UK
[c] Department of Physics, University of Patras, 26504 Patras, Greece
[d] Department of Electronic and Electrical Engineering, Faculty of Science and Engineering, University of Chester, Thornton Science Park, CH2 4NU, UK
[e] Department of Materials Science, University of Patras, 26504 Patras, Greece

† Corresponding author: Christos Tsonos; E-mail: tsonos@teilam.gr, Tel: +30 22310 60277, Fax: +302231033945

matrix can lead to the formation of conducting and magnetic hybrid nanocomposites [14]; however, polymer-based composites with high filler content (upto 60wt% in reported literature) have technical bottlenecks in meeting with the criterion of thin and light weight requirements for microwave absorbers, severely limiting their processability at large scale and the flexibility of the resulting material [16].

In this work, ternary polymer-based nanocomposites of PVDF/Fe_3O_4/CNT and PVDF/Fe_3O_4/GN, have been synthesized *via* twin screw compounding method and their microwave dielectric properties have been investigated. To the best of our knowledge, despite the low filler content (22 wt%) and low thickness of these systems, the microwave electromagnetic absorption properties are impressive; for example, *RL* of -28.8 dB at 5.6 GHz (for PVDF/Fe_3O_4/CNT, 0.7 mm thick) and -22.6 dB at 5.4 GHz (for PVDF/Fe_3O_4/GN, 0.9 mm thick) which are similar to those reported to other similar polymer nanocomposites [3, 7, 8]. The high EM shielding efficiency is attributed to the microwave absorption from magnetic effects of nano-sized Fe_3O_4 spinal ferrite and synergistic effects from multiple components and interfaces. Additionally, the use of dielectric PVDF as the polymer matrix with its excellent chemical corrosion resistance and high mechanical strength provides these ternary composites with the advantages of strong absorption, small thickness and flexibility for use promising EM wave absorber.

Materials & methods

PVDF homopolymer, SOLEF 1008 (from Solvay Solexis) was used for the production of nanocomposite samples. The polymer has a melt flow index (MFI) of 8 g/10 min at 230°C (under a load of 2.16 kg). Multiwalled CNT with a mean outer diameter of <10 nm, length of 10-30 µm, purity >90% (wt%) and GN powders with lateral dimensions of 1-2 µm with an average thickness of <4 nm and purity >99% (wt%), were obtained from Cheap Tubes Inc. (USA). Fe_3O_4 nanopowder was obtained from Aldrich with average particle size <50 nm and purity >98%. PVDF was compounded with nanofillers using a lab scale twin screw compounder (Thermo Scientific). Samples were composed of PVDF with suitable additives (CNT/GN, Fe_3O_4) in the loading range of 7 wt% (CNT/GN) and 15 wt% Fe_3O_4. As the content of the fillers was high, the compounding was done in a two-pass arrangement where a suitable amount (usually 50 wt% of the total filler content) of CNT/GN and Fe_3O_4 powders were compounded first, while in the second pass the rest of the amount was added [18]. The preparation of samples was carried out using a hot-press (sample size 50 g) at a pressure of 40kg/cm^2 for duration of 2 min 30 sec and then allowed to cool down at the same pressure using a cold press which rapidly cooled down the samples to room temperature, thereby providing samples of dimensions 170 mm x 170 mm and 1.0 mm thickness. Further details of the process can be found in our previous work [18]. The materials were characterized by X-ray diffraction (XRD, Philips PW 1050/25). The surface topography was examined using a Field Emission Scanning Electron Microscopy (FE-SEM, Jeol JSM-7401F). The electromagnetic parameters were measured by using a vector network analyzer (PNA-L N5230C) and analyzed based on the method described in previous references [19, 20].

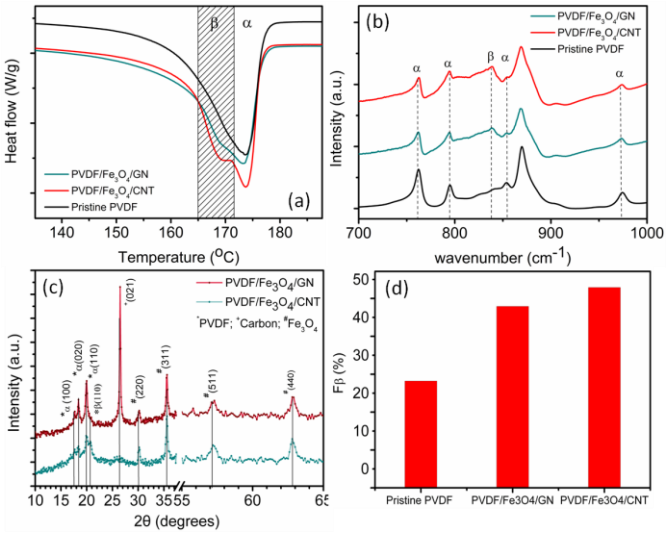

Fig. 1: (a) DSC analysis of the pristine PVDF and PVDF/Fe3O4/CNT, GN composites showing the melting behaviour and classification of α, β phases, (b) FTIR analysis showing the crystallisation of β phase in the composites with (d) the corresponding percentage, (c) XRD patterns of PVDF/Fe3O4/CNT and PVDF/Fe3O4/GN.

Results and discussion

The differential scanning calorimetry thermograms for pristine PVDF and PVDF/Fe_3O_4/CNT, PVDF/Fe_3O_4/GN composites are shown in Fig. 1(a). The samples show the melting temperature, T_M, in the range of 165-175ºC, with shoulder-like structures appearing at low temperature sides for the composite samples. While the T_M of the pristine PVDF sample is 173.8ºC; upon the composite formation with Fe_3O_4 and CNT/GN, low-temperature shoulder is observed at approximately 169ºC which can be attributed to the enhanced β-phase content and is further corroborated by the FTIR measurements. It is largely accepted in the literature that the melting peaks in the range 165-172°C correspond to the β-phase; while that in the range 172-175°C are consistent with the presence of α-phase crystals; with the further shoulder observed between 175 and 180°C being attributed to the γ-phase [21, 22]. In Fig. 2(a), it can be clearly observed that the addition of Fe_3O_4/CNTs seems to promote the formation of crystalline β phase as compared to the addition of Fe_3O_4/GN, as evident by the much more significant shoulder for PVDF/Fe_3O_4/CNT composite. The total crystallinity of samples, ΔX_C, can be calculated by assuming the fusion heat of 100% crystalline PVDF to be 104.7 J/g [21, 22]:

$$\Delta Xc = \frac{\Delta H_m}{\Delta H_{m100}} \times 100\% \qquad (1)$$

where ΔH_m and ΔH_{m100} are the melting enthalpy of the sample and the melting enthalpy for a 100% crystalline sample, respectively. As compared to the pristine PVDF (38.6%), only a marginal increase in the crystallinity was observed in the

Fe_3O_4/GN (38.2%) and Fe_3O_4/CNT (41.03%) samples and is similar to the values reported earlier [18]. To calculate relative amount of β phase in the composite film, FTIR spectra for pristine and the nanocomposite samples was collected, as shown in Figure 2(b). Various characteristic absorption bands, corresponding to the individual crystalline phases of the PVDF have been reported in the literature [18, 19]. As shown in Figure 2(b), absorbance bands at 760, 795, 853 and 974 cm^{-1}, correspond to α phases; while bands at 840, 878 and 1279 cm^{-1} corresponded to β phase. The content fraction of β phase in each sample of PVDF nanocomposites, *F(β)* was calculated according to Equation 1 [21, 22]:

$$F_\beta = \frac{A_\beta}{1.26A_\alpha + A_\beta} \times 100\% \qquad (2)$$

where A_α and A_β are crystalline mass fractions of α and β phases and, A_α and A_β correspond to their absorbance at 760 and 840 cm^{-1} respectively. This relation gives the relative amount of α and β phases in composites assuming that only these phases are present and has been used extensively in the literature. As shown in Figure 2d, the β content calculated for pristine PVDF samples and composite samples shows a huge increase from approximately 28% (pristine PVDF) to 48% (for PVDF/Fe_3O_4/GN) to ~53% (for PVDF/Fe_3O_4/CNT) samples, signifying the effect of CNTs in promoting the β phase crystallization. Similar behaviour has been seen in PVDF based composites prepared by melt compounding, in which the incorporation of CNTs produced transformation of α phase into β phase [23, 24]. In our previous studies, we have observed that upon incorporation of Fe_3O_4 nanoparticles in the PVDF/CNT matrix, the β-phase increases gradually, up to a maximum value of 51% (10 wt% Fe_3O_4), beyond which it dropped off significantly to 39% with the addition of 15 wt% Fe3O4, thereby leading us to conclude that it is mainly CNTs which promote the formation of β phase in PVDF nanocomposites, while the influence of Fe_3O_4 is less important. The XRD patterns of PVDF based nanocomposites are presented in Figure 2(c). The first four peaks of the spectrum can be assigned to the PVDF matrix. In particular, the diffraction peaks at 2θ= 17.8°, 18.4° and 20.0° correspond to the (100), (020) and (110) planes of the α-phase of PVDF orthorhombic lattice respectively [25-28]. The weak diffraction peak at 2θ=20.7° indicates the presence of β-phase of PVDF [26]. Some blurry reflections near these peaks may indicate the existence of γ-crystals [27]. For the composite with CNT, two sharp peaks at 2θ= 17.8° and 18.4° have been merged into a broader peak, which can be explained due to the presence of CNT that affects α-phase crystals [26]. The rest of the peaks are contributed from the Fe_3O_4. Namely, 2θ= 30.1°, 35.5°, 43.3°, 57.2°and 62.8° correspond to the (220), (311), (400), (511) and (440) planes of the cubic spinel phase of Fe_3O_4 [29]. Compared to the peak feature for CNT particles, the rather sharp feature at 26.5° for the composite with GN particles, corresponding to the (002) graphitic plane is significantly higher. This can be attributed to the formation of short range order in stacked graphene sheets owing to the high pressures

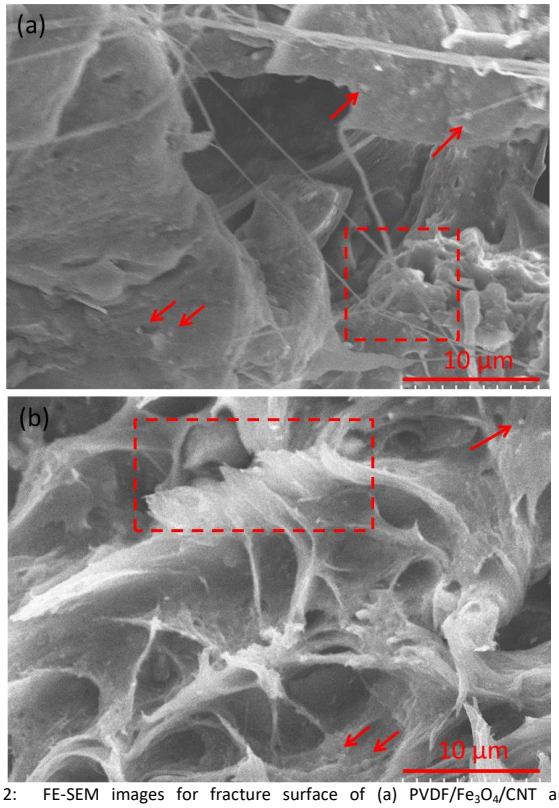

Figure 2: FE-SEM images for fracture surface of (a) PVDF/Fe_3O_4/CNT and (b) PVDF/Fe_3O_4/GN samples.

(40 kg/cm^2) and high temperatures used in the hot-press process [30]. Due to the manufacturing process, some agglomeration of the graphene sheets occurs and exists within the composites with the graphene sheet still maintaining their flake-like structure (Fig. 2(b)). The SEM fracture images shown in Figure 2(a, b) reveals a good dispersion of the CNT and GN nanoinclusions (dotted squares in Fig. 2(a, b)) in the PVDF matrix. At the given magnifications, while it was not possible to view the individual nanoparticles, some agglomerates of the Fe_3O_4 nanoparticles could be observed clearly (marked arrows in Fig. 2(a, b)). The measurements of complex permittivity (ε*=ε′−jε″) and permeability (μ*=μ′−jμ″) was carried out in the range of 3-10 GHz for both the PVDF/Fe_3O_4/CNT and PVDF/Fe_3O_4/GN nanocomposites and are presented in Figures 3a, b. In Fig. 3a, the PVDF/Fe_3O_4/GN nanocomposite presents relatively higher ε′ values than PVDF/Fe_3O_4/CNT, while the real part of permittivity ε′ for both nanocomposites gradually decreases from 9.0 to 5.1, and from 8.0 to 2.6 respectively as the frequency increases from 3 to 10 GHz. However, their imaginary part ε″, increases slightly as the frequency increases. It is clear that the PVDF/Fe_3O_4/CNT sample presents approximately 2.2 times higher dielectric losses in the measured frequency range. As shown in Fig. 3b, the PVDF/Fe_3O_4/CNT sample exhibits relatively higher μ′ and μ″ values. It is possible that for unpurified CNTs used in this study, the residual catalyst (~10 wt% according to the manufacturer), largely consisting of magnetic transition elements (Fe, Co, Ni etc.) can play a part in enhancing the permeability values for PVDF/Fe_3O_4/CNT as compared to the PVDF/Fe_3O_4/GN samples

which do not have any residual catalyst material [31]. Similarly, μ′ values gradually decrease as the frequency increases, however, μ″ values gradually increase as the frequencies increase for both nanocomposites. It should be noted here that the μ″, which is related to the magnetic energy losses is significantly higher than μ′, which is related to the magnetic energy stored. The fact is demonstrated by both the nanocomposites. In order to compare microwave absorption properties of the nanocomposites, the reflection loss (RL) was calculated according to the transmission line theory [32], by the following equation:

$$RL(dB) = 20\log\left|\frac{Z_{in}-1}{Z_{in}+1}\right| \quad (3)$$

where the normalized input impedance (Zin) is given by the relation

$$Z_{in} = \sqrt{\frac{\mu^*}{\varepsilon^*}}\tanh\left[j\left(\frac{2\pi fd}{c}\right)\sqrt{\mu^*\varepsilon^*}\right] \quad (4)$$

where ε*=ε′−jε″, μ*=μ′−jμ″, f is the microwave frequency (Hz), d is the thickness of the absorber (m), and c is the velocity of light in free space (m/s).

The variations of RL at different sample thickness d (0.7, 0.8, 0.9, 1.0 and 1.2 mm) were calculated and shown in Figures 3a-b. Both nanocomposites showed a minimum RL peak which is shifted to lower frequencies while their magnitude is slightly reduced when the thickness increases. PVDF/Fe_3O_4/CNT sample with d = 0.7 mm demonstrated the best absorption properties, for example a minimum of -28.8 dB RL at 5.6 GHz, beyond -10 dB loss through the whole measurement X band. The absorption bandwidth, i.e. the frequency range exceeding -20 dB (over 99% absorption), is 2.3 GHz (4.4-6.7 GHz). As the sample thickness increases from 0.7 to 1.2 mm, the absorption properties of PVDF/Fe_3O_4/CNT seem to be extended into the range lower than 3 GHz. This superior and excellent absorption ability does not stand only for this kind of nanocomposite, as the PVDF/Fe_3O_4/GN with d = 0.9 mm, presents a minimum RL of -22.6 dB at 5.4 GHz and -10 dB RL through the whole measurement frequencies, however, the absorption bandwidth, is 1.4 GHz (4.8-6.2 GHz). Also, for d = 0.7 mm PVDF/Fe_3O_4/GN sample it shows a minimum RL value of -24.1 dB at 7 GHz, the better absorption bandwidth exceeding -20 dB where is 2.5 GHz (6.0-8.5 GHz), while all the RL values in the frequency range 3.8-10 GHz are lower than -10 dB and this bandwidth seems to extend much higher than 10 GHz.

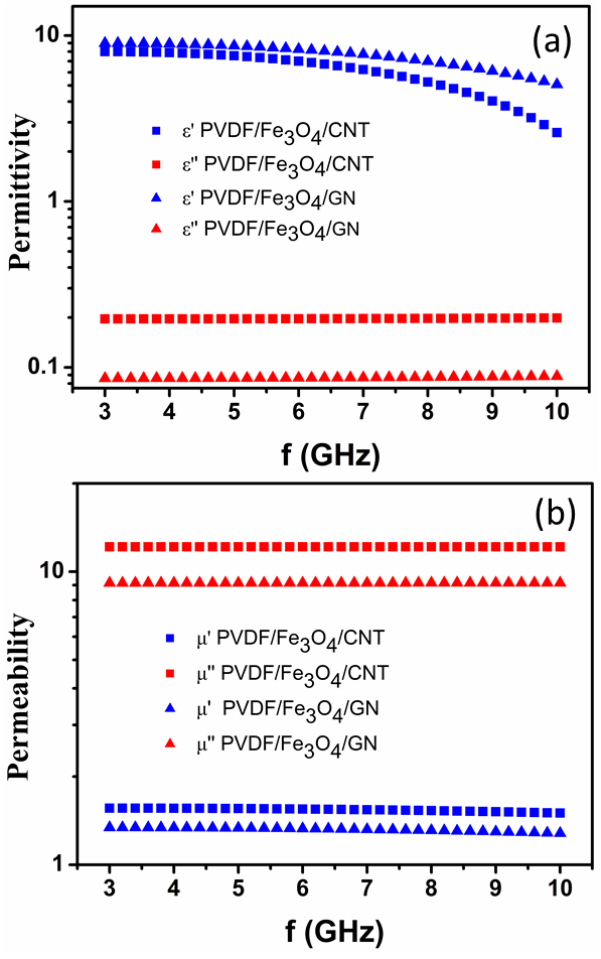

Fig. 3: Real and imaginary parts of complex permittivity ε* (a) and complex permeability μ* (b), for PVDF/Fe_3O_4/CNT and PVDF/Fe_3O_4/GN.

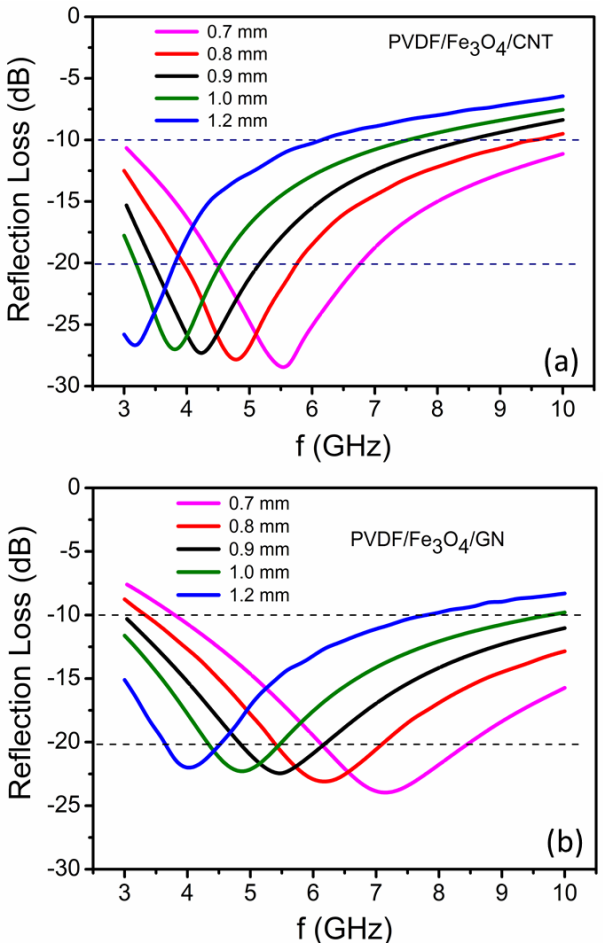

Fig. 4: Reflection loss curves of (a) PVDF/Fe3O4/CNT and (b) PVDF/Fe3O4/GN samples.

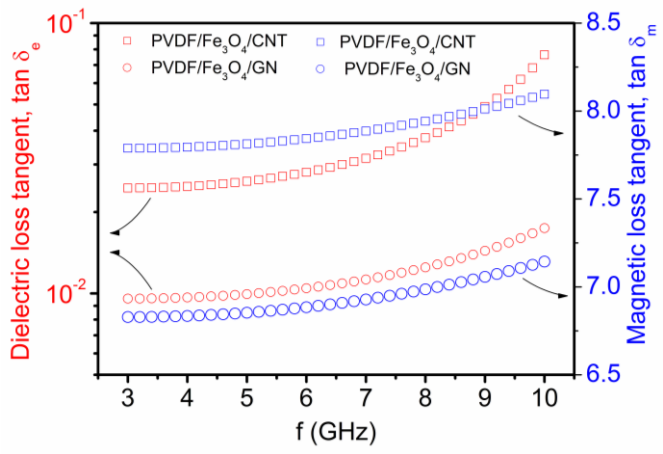

Fig. 5: Dielectric and magnetic loss tangents of the PVDF/Fe3O4/CNT and PVDF/Fe3O4/GN samples.

Generally, multi-interfaces between the components of the composites can serve as polarized center, which contributes to EM wave absorption properties due to the induced interfacial polarization [33]. The dielectric and magnetic losses for these composites can be evaluated by the dielectric loss (tan δ_e = ε”/ε’) and magnetic loss (tan δ_m = μ”/μ’) tangent values. For the PVDF/Fe_3O_4/CNT system, the dielectric loss tangent values vary between 0.02-0.07, while the corresponding magnetic loss tangent varies between7.80-8.10; the corresponding values for the PVDF/Fe_3O_4/GN system varies between 0.009-0.017 (for tan δ_e) and 6.80-7.15 (tan δ_m), Fig. 5. However, the relatively low value of dielectric loss (in the lower frequency range of 3-8 GHz) suggests that this mechanism is not crucial to the EM absorption properties in the two ternary systems studied here. Beyond the value of 8 GHz, it seems that the value of dielectric loss tangent is increasing rapidly, while the value of magnetic loss is relatively consistent (Fig. 5). Similar results of magnetic loss dominated EM wave attenuation in the low frequency region and dielectric loss dominated attenuation in the high frequency region has been reported by Liu et al in their study of carbon encapsulated magnetite nanospindle PVDF composites [15]. It is clear observed that PVDF/Fe_3O_4/CNT sample presents a better absorbing property compared with the other sample, PVDF/Fe_3O_4/GN. The significantly high magnetic loss as shown in Fig. 3b for of both nanocomposites, suggests that the microwave absorption results mainly from magnetic rather than electric effects, which can be ascribed eddy current, natural resonance and exchange resonance effects [15, 30]. This is further corroborated by the fact that the RL peaks for these samples (Fig. 4(a, b)) were all observed in the low-frequency region, whereas for the dielectric loss dominated mechanism, the peaks are shifted to the higher frequency region [16, 34]. For the PVDF/Fe_3O_4/CNT and PVDF/Fe_3O_4/GN composites, the magnetic loss is caused by the time lag of the magnetisation vector **M** behind the magnetic field vector **H**. In the microwave region, the motion of the magnetization vector M cannot keep up with the applied field, which results in the occurrence of μ” [15]. For both the samples, the permeability values (μ” and μ’) do not show any strong trends/variation with the change in the frequency. In fact, both the real and imaginary parts of the permeability seem almost independent of the frequency. This phenomenon can be explained by the insulation effect provided by the carbonaceous additives (CNT, GN) [35]. It is well known that the addition of insulating graphitic shell improves the high-frequency performance of soft magnetic materials like Fe, Ni etc. For the metallic magnetic materials like magnetite, the low cut-off frequency (<1.5 GHz for bulk magnetite) is related to the eddy currents induced by the alternating current field, due to poor insulation between the particles [35]. These eddy currents especially at high frequency can lead to significant losses via heating of the material. In the case where no CNTs/GN is present, then the formation of a continuous Fe_3O_4 nanoparticle network will lead to creation of eddy currents causing μ’ to decrease with frequency rapidly and the imaginary part μ” would reach a maximum at a lower frequency [36]. In the present system, the almost constant values of μ’ and μ” indicate good insulation between the metal nanoparticles via the addition of GN and CNTs. The measured complex permittivity and permeability are not able to fully explain the loss mechanisms from the microstructures of nanocomposites. However, one possible reason is the surface phenomena near Fe_3O_4-CNT/PVDF and Fe_3O_4-GN/PVDF interfaces. These kinds of interfaces are characterized by the relation of charge-carrier transport in the conductor and the spin ordering of the magnetic phase [37]. However, the intrinsic large magnetic loss of ferrite particles is the crucial contribution factor to this large loss phenomenon as Fe_3O_4 shows highest magnetic losses in relation to other nano-sized spinal ferrites [38] and moreover, coupling and interfacing effects between Fe_3O_4, CNT/PVDF and GN/PVDF could be responsible for superior EM absorbing characteristics of both nanocomposites. Finally, from the engineering point of view, the superior EM absorption properties of the two ternary nanocomposites systems, can be contributed from the impedance matching conditions. According to Eqs. 3, 4, the combination of the six parameters ε`, ε``, μ`, μ``, *f*, *d*, has acquired the normalized input impedance to take value Z_{in} ~ 1 .

Conclusions

Two ternary nanocomposite systems, PVDF/Fe_3O_4/CNT and PVDF/Fe_3O_4/GN, were prepared with twin screw compounding method. The conductive inclusions CNT/GN together with magnetic Fe_3O_4 particles were kept at the same levels of 7 and 15 wt%, respectively. Both nanocomposites exhibit excellent and superior EM absorption properties which are attributed to the dominant magnetic losses. Dielectric loss is significant lower than the magnetic loss, which is a very important and desirable property as it leads to low dielectric heating. PVDF/Fe_3O_4/CNT with d = 0.7 mm presents a minimum RL value of -28.8 dB at 5.6 GHz and broad band loss below than -10 dB. Similarly, PVDF/Fe_3O_4/GN sample with d = 0.9 mm, presents a minimum RL of -22.6 dB at 5.4 GHz and broad band

absorption properties. The results indicate that both ternary nanocomposites with realistic thin thickness close and around 1 mm, can be used as an attractive candidate for EM absorption materials in the microwave regions.

Acknowledgements

Materials support from Solvay Speciality Polymers is greatly acknowledged. This research has been co-financed by the European Union (European Social Fund – ESF) and Greek national funds through the Operational Program 'Education and Lifelong Learning' of the National Strategic Reference Framework (NSRF) Research Funding Program: THALES. Investing in knowledge society through the European Social Fund (MIS 379346).

References

1 X. Tang and K. A. Hu, *Mater Sci Eng B*, 2007, **139**, 119-123.
2 Y. Huang, L. Wang and X. Sun, *Mater Lett,* 2015*,* **144**, 26-9.
3 P. Liu, Y. Huang and X. Zhang, *Mater Lett,* 2014, **136**, 298-301.
4 L. Wang X. Jia, Y. Li, F. Yang, L. Zhang, L. Liu, X. Ren and H. Yang, *J Mater Chem A,* 2014, **2**, 14940-6.
5 L. D. C. Folgueras, E. L. Nohara, R. Faez and M. C. Rezende, *Mat Res,* 2007*,* **10,** 95-9.
6 J. Huo, L. Wang and H. Yu, *J Mater Sci,* 2009, **44,** 3917-27.
7 P. Liu, Y. Huang and X. Zhang, *Mater Lett,* 2014, **129**, 35-8.
8 Y. F. Zhu, Q. Q. Ni, Y. Q. Fu and T. Natsuki, *J Nanopart Res*, 2013, **15,** 1-11.
9 X. J. Zhang, G. C. Lv, G. S. Wang, T. Y. Bai, J. K. Qu, X. F. Liu and P. G. Yin, *RSC Adv*, 2015, **5,** 55468-73.
10 S. H. Ahmad, M. H. Abdullah, D. Hui, A. N. Yusoff and D. Puryanti, *J Magn Magn Mater,* 2010, **322**, 3401-9.
11 J. Xie, M. Han, L. Chen, R. Kuang and L. Deng, *J Magn Magn Mater*, 2007, **314***,* 37-42.
12 X. G. Liu, D. Y. Geng, H. Meng, P. J. Shang and Z. D. Zhang, *Appl Phys Lett,* 2008, **92,** 173117
13 H. Xu, L. Hu, S. M. Anlage and G. Gruner, *Appl Phys Lett*, 2007, **90,** 183119
14 C. Yang, H. Li, D. Xiong and Z. Cao, *React Funct Polym*, 2009, **69,** 137-44.
15 X. Liu, X. Cui, Y. Chen, X. J. Zhang, R. Yu, G. S. Wang and H. Ma, *Carbon*, 2015, **95**, 870-878
16 X. Liu, Y. Chen, X. Cui, M. Zeng, R. Yu, and G. S. Wang, *J Mater Chem, A,*2015, **3**, 12197-12204.
17 G. S. Wang, X. J. Zhang, Y. Z. Wei, S. He, L. Guo and M. S. Cao, *J Mater Chem A*, 2013, **1**, 7031-7036.
18 C. Tsonos, C. Pandis, N. Soin, D. Sakellari, E. Myrovali, S. Kripotou, A. Kanapitsas and E. Siores, *Express Polym Lett,* 2015, **9**, 1104-18.
19 B. Yang, R. J. Wylde, D. H. Martin, P. Goy, R. S. Donnan and S. Caroopen, *IEEE T Microw Theory,* 2010, **58**, 3587-97.
20 L. Zhu, Y. Wang, F. Hu and H. Song, *Appl Surf Sci*, 2015, **345,** 349-54.
21 N. Soin, D. Boyer, K. Prashanthi, S. Sharma, A. A. Narasimulu, J. Luo, T. H. Shah, E. Siores and T. Thundat, *Chem Comm*, 2015, **51**, 8257-8260.
22 N. Soin, T. H. Shah, S. C. Anand, J. Geng, W. Pornwannachai, P. Mandal, S. Sharma, R. L. Hadimani, D. V. Bayramol and E. Siores, *Energy & Environ Sci*, 2014, **7**, 1670-1679.
23 K. Ke, P. Pötschke, D. Jehnichen, D. Fischer, and B. Voit, *Polymer*, 2014, **55**, 611-619.
24 G. Georgousis, C. Pandis, A. Kalamiotis, P. Georgiopoulos, A. Kyritsis, E. P. Pissis, M. Micusik and M. Omastova, *Compos Part B-Eng*, 2014, **68**, 162-169.
25 X. Liu, H. J. Chen, B. Yang, X. Chen, C. Parini and D. Wen, *J Infrared Millim Tech.,* 2013, **34**, 140-51.
26 S. Vidhate, A. Shaito, J. Chung and N. A. D'Souza, *J Appl Polym Sci,* 2009, **112,** 254-60.
27 M. Muthuvinayagam and C. Gopinathan, *Polymer*, 2015, **68,** 122-30.
28 G. Gao, Q. Zhang, X. B. Cheng, R. Sun, J. G. Shapter, T. Yin and D. Cui, *J Alloy Compd*, 2015, **649,** 82-8.
29 S. Li, Y. Gong, Y. Yang, C. He, L. Hu, L. Zhu, L. Sun and D. Shu, *Chem Eng J,* 2015, **260,** 231-9.
30 G. Wang, Z. Gao, G. Wan, S. Lin, P. Yang, and Y. Qin, *Nano Res.* 2014, **7**, 704-716.
31 R. Che, L. M. Peng, X. F. Duan, Q. Chen, and X. L. Liang, *Adv. Mater.,* 2004, **16**, 401-405.
32 S. S. Kim, S. B. Jo, K. I. Gueon, K. K. Choi, J. M. Kim and K. S. Churn, *IEEE T Magn,* 1991, **27,** 5462-4.
33 Y. J. Chen, F. Zhang, G. G. Zhao, H. B. Jin, P. Gao, C.-L. Zhu, L. Zhu, M.–S. Cao and G. Xiao et al. *J Phys Chem C,* 2010, **114,** 9239–44.
34 D. P. Sun, Q. Zou, Y. P. Wang, Y. J. Wang, W. Jiang and F. S. Li, *Nanoscale*, 2014, **6**, 6557-6562.
35 X. G. Liu, B. Li, D. Y. Geng, W. B. Cui, F. Yang, Z. G. Xie, D. J. Kang and Z. D. Zhang, *Carbon*, 2009, **47**, 470-474.
36 W. Liu, W. Zhong, H. Y. Jiang, N. J. Tang, X. L. Wu, W. Y. Du, *Eur. Phys. J B*, 2005, **46**, 471-474.
37 Y. H. Chu, L. W. Martin, M. B. Holcomb, M. Gajek, S. J. Han, Q. He, N. Balke, C.-H. Yang, D. Lee, W. Hu W, Q. Zhan, P.-L. Yang, A. Fraile-Rodríguez, A. Scholl, S. X. Wang and R. Ramesh, *Nat Mater,* 2008, **7,** 478-82.
38 S. Duggal and G. D. Aul, *Int J Eng Adv Tech,* 2014, **3***,* 12-9.

